

emitter Tx, silicon-on-sapphire detector Rx, fs laser source) in whose THz beam path a THz surface waveguide is located. The particular setup is described in detail by Gong et al. [9]. The THz wave is coupled into a parallel-plate waveguide using silicon optics. A THz surface wave is launched by metal flare coupling at the exit face. The advantage of this layout is that the THz pulse is guided on top of the metal sheet, being less sensitive to environmental influences compared to pure free-space geometries. Independent of the layer T to be investigated, there is already a $12.5\ \mu\text{m}$ thick dielectric coating S on the top of the metal sheet. This reduces the THz evanescent field extent into free-space considerably, reducing the exponential fall-off of the electric field in z-direction from the cm to mm range [9]. So, the wave has much tighter guiding and therefore shows less leakage and diffraction. The field solution of the coated metal sheet is identical with that of a dielectric slab of twice the thickness, because the metal acts like a mirror for the THz wave. As the dielectric coating S has a thickness of only a small fraction of the wavelength, most of the guided THz wave is outside of the dielectric. So the field forms a "line focus" in the z-direction with propagation in the x-direction. In the y-direction diffraction limited divergence is expected.

In order to understand the extent and the field coupling of the THz surface wave on top of the dielectric coated metal sheet, the transmission through a 3 mm-thick metal slit on top of the guide was compared to the 32 mm diameter aluminum cylinder, separately measured as a function of the approach distance d. The results are shown in Fig. 2. The propagation distance from the cylinder or slit to the receiver (as shown in Fig. 1) was 8 cm, in order to detect only the propagating wave without diffracted contributions. The surface wave is expected to have an exponential decay of the evanescent electric field given by $e^{-\alpha z}$ with $\alpha = 0.76\ \text{mm}^{-1}$ for a frequency of 0.5 THz [9]. Introducing the slit into the wave spatially truncates the input intensity profile. For further propagation after this interaction, the major fraction of the transmitted power is re-captured by the surface wave. So, when the cylinder or slit enters the surface wave, the amplitude transmission drops from 1 (normalized to a surface wave without interacting object) to smaller values in a monotonic manner. The small modulations for the approaching cylinder at 0.8 THz and 1.8 THz are caused by interference and dispersion, which slightly change the THz pulse width and is thereby seen in this type of data evaluation (peak-to-peak of transmitted electric field).

In the 3 mm-thick slit case, at direct contact (0 mm distance from dielectric coating S), there is still a small transmission observable (approximately 20% electric field, 4% intensity). The reason is that a fraction of the wave is guided spatially within the dielectric. For the round surface of the cylinder, the transmission at contact is much higher (55% electric field, 30% intensity). The reason for this increase is that, when the propagating surface wave enters the gently changing interaction area, the mode profile changes adiabatically. Firstly, its spatial extent follows the separation between the two metallic surfaces (cylinder and sheet), and secondly the mode shape monotonically changes from an exponential decay in z-direction to a roughly homogeneous field distribution at contact point. This can be done efficiently if the changes of THz beam extent are introduced adiabatically, i. e. slowly varying with respect to the wavelength. The process is similar to our previous results obtained for free-space coupling using metal flares [10], where the THz wave could squeeze through the smooth gap with only minor reflection losses. So a very intense field concentration propagates through the point of minimal distance d between the cylinder and the sheet, allowing highly sensitive measurements of thin sample layers.

3. Results and Discussion

In the traditional single-pass case, when a free-space THz pulse propagates through a sheet of thickness T and refractive index n, a pulse delay δt is caused with respect to a free-space

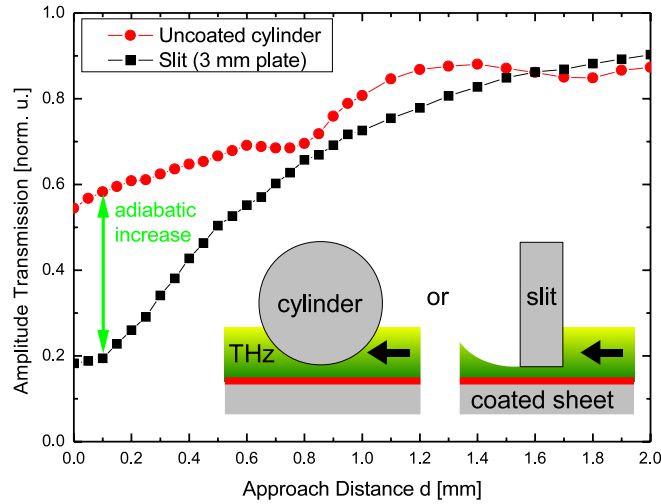


Fig. 2. Comparison of THz amplitude transmission for a 32mm diameter aluminum cylinder and a 3mm-thick metal plate slit on top of the dielectric coated waveguide. For small approach distances the round cylinder gives rise to a higher transmission than the slit, the adiabatic increase.

reference ($n = 1$) given by

$$\delta t = \frac{(n - 1)T}{c}, \quad (1)$$

for which c is the speed of light. So an accurate thickness measurement requires a precise pulse delay measurement. For the experiment described here, a guided wave setup using the high filling factor of a THz parallel-plate waveguide (PPWG) [11] is proposed and demonstrated to increase the detection sensitivity.

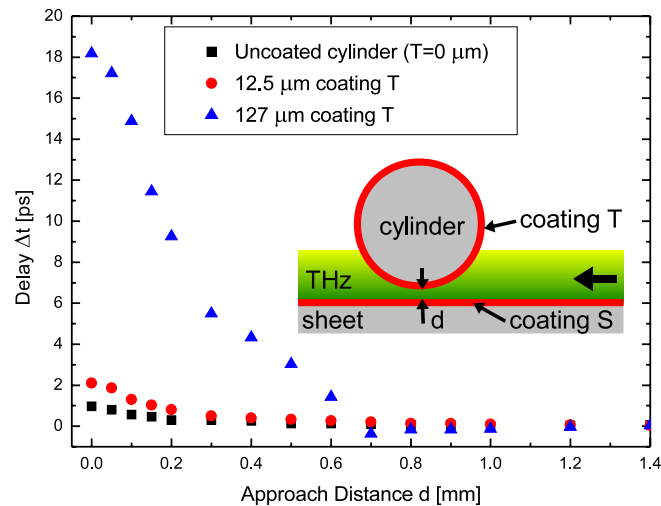


Fig. 3. Measured delay for an uncoated, a 12.5 μm and a 127 μm (Parafilm® M) coated, 32 mm diameter metal cylinders as a function of the approach distance d .

In Fig. 3 the measured pulse delays for different approach distances and samples (all $n = 1.5$) are shown. The values are normalized to zero for the undisturbed WG. The delay changes significantly as the cylinder enters the surface wave ($1/e$ width 1.3 mm, large delay change below 0.7 mm approach distance). The closer the cylinder gets, the larger is the delay, due to the higher filling factor and the larger effective refractive index n_{eff} . The delay increases as the cylinder approaches the surface, giving the maximum delay in contact ($d = 0$). Also the thicker coating gives a larger delay. Even for an uncoated cylinder, some delay is observed, roughly half that of the $12.5 \mu\text{m}$ coated cylinder. The reason is that the uncoated cylinder compresses the evanescent field of the surface WG into the dielectric coating S (also $12.5 \mu\text{m}$). In order to separate the effect of the uncoated cylinder and the surface WG on the thickness measurement itself, the following values are normalized to the uncoated cylinder in contact.

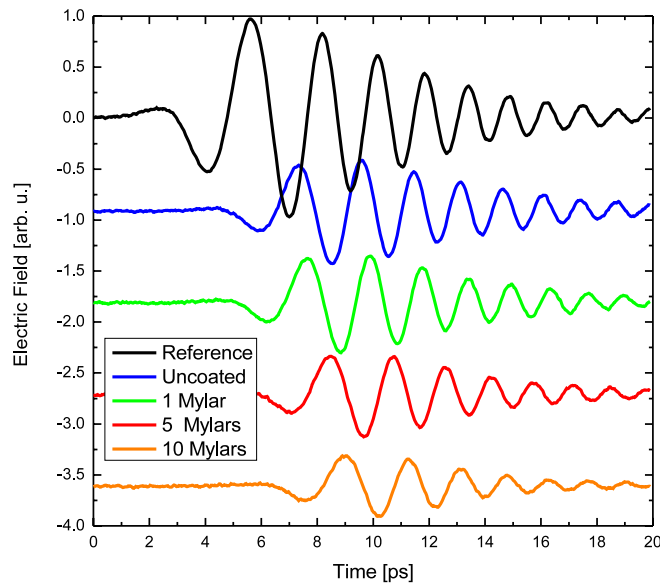


Fig. 4. The measured reference electric field (upper trace) is for the undisturbed THz surface wave, the uncoated electric field is for the uncoated 32 mm diameter aluminum cylinder. Stepwise layers of PET plastic sheet (Mylar® with $2.5 \mu\text{m}$ thickness) are attached, shown here for 1, 5 and 10 layers, offset for clarity. All cylinders are in contact.

The high sensitivity of the setup is demonstrated for very thin multiple layers of Mylar® wrapped on a 32 mm diameter cylinder. The particular plastic is biaxially-oriented polyethylene terephthalate ($n_{\text{PET}} = 1.7$) with a thickness of $2.5 \mu\text{m}$ (according to specification sheet and mechanically measured 64 layer stack $160 \pm 10 \mu\text{m}$). The recorded electric fields are plotted in Fig. 4. The measured THz reference pulse is the undisturbed THz field from the $12.5 \mu\text{m}$ dielectric layer THz surface wave (DL-TSW, see Ref. [9]). This pulse consists of a rapidly decaying, chirped, sinusoidal oscillation, where the highest frequency components go the slowest. The center frequency is around 500 GHz. Obviously, the thicker the coating gets, the more each trace is delayed. As we are dealing with broadband THz pulses, where the bandwidth and the frequency come into the same range, the concepts of envelope and carrier frequency, respectively group and phase velocity, are difficult to apply. The leading edge of the positively chirped pulse train can be easily evaluated and is less sensitive to pulse forming effects. Consequently, to evaluate the pulse delay, the first zero crossing after the main maximum of the multi-cycle pulse is the measured quantity. This is determined with a high accuracy and is less dependent

on noise and pulse shape than the maximum.

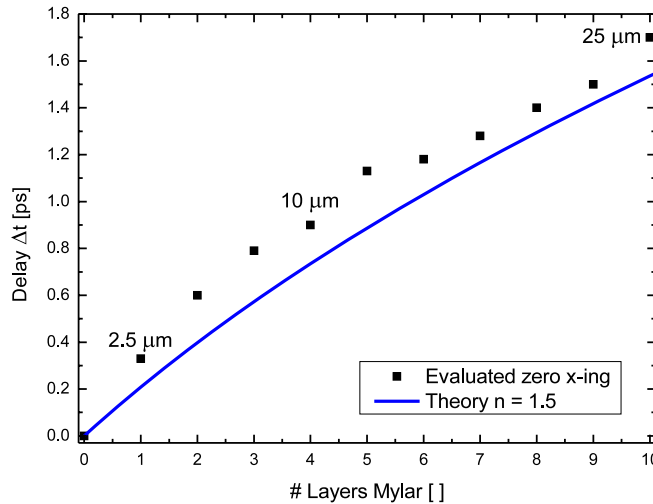


Fig. 5. Delay at contact caused by the 32mm diameter aluminum cylinder on which step-wise layers of Mylar® are attached.

Figure 5 shows the contact delay for a series of cylinders, from uncoated to 25 μm coating, along with the corresponding theory curve to be introduced later. Clearly each additional 2.5 μm layer can be identified. The slope of the plot is steep in the beginning, then showing a slow transition to saturation. This is expected as the filling factor has to be regarded as an integrated value over the entire interaction distance with the surface wave. So, once the waveguide is filled, only smaller contributions come from the filling factor during the compression and expansion of the guided surface wave. The given theory curve slightly underestimates the expected delay, because in the simulations both refractive indices were considered to be 1.5.

4. Theory and Simulation

A simple theoretical model, regarding the input surface wave as a constant field with an extent of 1 mm, gives an understanding in reasonable agreement with the experiment. For the interaction between the cylinder and the surface wave, the conditions of a partially-filled PPWG are given. The input field is assumed to couple adiabatically into the lowest order propagating mode. A good approximation to the lowest order solution for the wave propagation in a partially-filled PPWG is that the electric displacement field $D = \epsilon E$ is constant in the z -direction with the corresponding E -field changing abruptly at the dielectric interfaces with a ratio of $\epsilon = n^2$ [12]. So the energy distribution in the mode defines the effective refractive index. The largest contribution to the delay is given at the contact point at which the energy distribution is completely within the dielectric coatings. Losses are not included in the adiabatically compressed model as they do not influence the observed delay.

Because the above picture was difficult to solve numerically for the time delay, we adapted the problem to the model known for partially-filled PPWGs [13] with only one incorporated sample layer of refractive index n . In our experimental setup, the overall dielectric layer thickness is given by the sum of the cylinder coating T and the coating S on the metal sheet. This approximation assumes that the propagation constant of a partially filled PPWG is not influenced by the position of the air gap in the guide. The displacement field $D = \epsilon E$ remains constant. To apply the standard PPWG equations a second assumption is made on the refractive index

of the cylinder's coating T being identical to the refractive index of the dielectric layer S of the waveguide ($n_S = n_T = n$). In terms of numbers, we regard the refractive index of the PET sample ($n_{PET} = 1.7$) being the same as that of PE ($n_{PET} = 1.5$).

Now applying the results of Gallot et. al. [13] the effective refractive index of the entire partially filled waveguide of our system is given by

$$n_{\text{eff}}(x) = \sqrt{\frac{1}{1 - \frac{T+S}{T+d(x)+S} \left(1 - \frac{1}{n^2}\right)}} \quad (2)$$

with n the refractive index calculations of the dielectric coating S, and $d(x)$ the air gap between the two layers changing during the propagation. Therefore, the effective refractive index is also depending on the coordinate x of wave propagation. To obtain the complete delay accumulated during the interaction (compression and expansion) an integration has to be performed

$$\Delta t = \int_{\text{interaction}} \frac{n_{\text{eff}}(x) - 1}{c} dx. \quad (3)$$

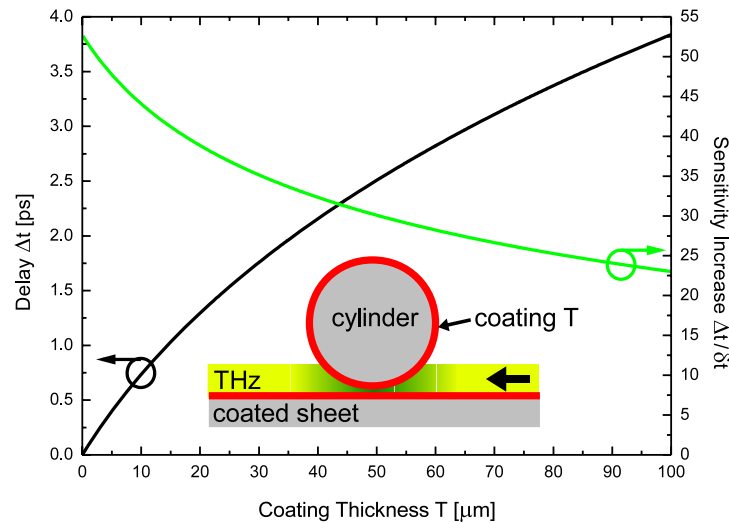


Fig. 6. Theoretically expected delay caused by dielectric coatings on a cylinder of 32 mm diameter in contact and within a homogeneous field of 1 mm extent (see inset sketch). The related sensitivity increase is calculated with respect to the single pass delay.

The effective refractive index was implemented in a MATLAB® program, where the total delay Δt is calculated as a discrete sum over the interaction between the cylinder and the surface wave according to Eq. (3). This is schematically depicted in the inset of Fig. 6. It also shows the simulated results for a 32 mm cylinder with different coatings in contact with the metal sheet ($d = 0 \mu\text{m}$). Again, the change of delay per micron added layer is the biggest for thin layers with a transition to saturation. The sensitivity increase $\Delta t/\delta t$ is defined as the calculated delay divided by the single pass delay according to Eq. (1) and (3). It is again the largest for very thin layers, with values around 40 for the experimentally investigated layers. These two plots show the useful working range of this approach: As typical resolvable delay changes are below 1 ps, typically 0.1 ps, the minimum resolvable coating thickness is less than $1 \mu\text{m}$.

Investigated thicker coatings (between $40\ \mu\text{m}$ and $100\ \mu\text{m}$) have also shown results corresponding to theory if dispersion is also included. But for those thicknesses, the sensitivity enhancement factor is not as high as for thin layers, and already single pass measurement can determine the thickness. So our new approach is advantageous if standard TDS loses its accuracy for very thin layers.

5. Conclusion

We have experimentally shown and simulated, how easy-to-use THz waveguide geometries can be used to enhance the sensitivity of layer thickness determination. The detection threshold for thin films was demonstrated to be at less than 2.5 microns for a plastic coating with refractive index of 1.7. This was achieved by using the high filling factor of a parallel-plate wave guide, where the upper half is the coated metal cylinder under test. The THz beam is adiabatically coupled similar to a horn antenna until it squeezes through the sub-wavelength gap. On this way, the interaction between the coating and the THz wave is immense, giving rise to a large delay with respect to the single pass value in the time domain. This high filling factor increased the observed delay by a factor of 50.

Acknowledgement

This work was partially supported by the National Science Foundation and the PROF.x²-research fellowship program of the Fraunhofer Gesellschaft.